Small hysteresis and giant magnetocaloric effect in Nb-substituted $(Mn,Fe)_2(P,Si)$ alloys

Hu, Shuyuan; Miao, Xuefei; Liu, Jun; Ou, Zhiqiang; Cong, Mengqi; Haschuluu, Oimod; Gong, Yuanyuan; Qian, Fengjiao; You, Yurong; Zhang, Yujing

DOI
10.1016/j.intermet.2019.106602

Publication date
2019

Document Version
Final published version

Published in
Intermetallics

Intermetallics 114 (2019) 106602

Contents lists available at ScienceDirect

Intermetallics

journal homepage: www.elsevier.com/locate/intermet

Small hysteresis and giant magnetocaloric effect in Nb-substituted (Mn,Fe)$_2$(P,Si) alloys

Shuyuan Hu[a], Xuefei Miao[a,*], Jun Liu[a,b], Zhiqiang Ou[c], Mengqi Cong[d], Oimod Haschuluu[c], Yuanyuan Gong[a], Fengjiao Qian[e], Yurong You[a], Yujing Zhang[a], Feng Xu[a,**], Ekkes Brück[b]

[a] MIIT Key Laboratory of Advanced Metallic and Intermetallic Materials Technology, School of Materials Science and Engineering, Nanjing University of Science and Technology, 210094, Nanjing, China
[b] Fundamental Aspects of Materials and Energy, Department of Radiation Science and Technology, Delft University of Technology, Mekelweg 15, 2629, JB Delft, the Netherlands
[c] Inner Mongolia Key Laboratory for Physics and Chemistry of Functional Materials, Inner Mongolia Normal University, 010022, Hohhot, China
[d] Key Laboratory of Advanced Materials Design and Additive Manufacturing of Jiangsu Province, Jiangsu University of Technology, 213001, Changzhou, China
[e] College of Physics, Nanjing University of Aeronautics and Astronautics, 210016, Nanjing, China

ARTICLE INFO

Keywords:
Functional alloys
Magnetic properties
Phase transformation
Mechanical alloying and milling
Microstructure
Energy systems

ABSTRACT

The influence of Nb substitution on the structure, magnetoelastic transition and magnetocaloric properties has been investigated for the $Mn_{1.1}Fe_{0.85-x}Nb_xP_{0.43}Si_{0.57}$ alloys. The substitution for Fe by merely 4.7 at.% Nb (i.e. $x = 0.04$) significantly diminishes the thermal hysteresis from 10 to 1 K due to the reduced structural discontinuity crossing the magnetoelastic transition. This also improves the mechanical stability. The Curie temperature of the magnetoelastic transition is lowered by approximately 11.6 K per at.% of the Nb substitution, originating from the enhanced covalent bonding that favors the paramagnetic state. The giant magnetocaloric effect is still retained in the Nb-substituted alloys.

1. Introduction

The (Mn,Fe)$_2$(P,Si) alloys, evolving from the (Mn,Fe)$_2$(P,As) via replacing the toxic element arsenic by the nontoxic and inexpensive element silicon [1,2], retain the giant magnetocaloric effect (MCE) observed in the latter [3]. The (Mn,Fe)$_2$(P,Si) alloys crystallize in the hexagonal Fe_2P-type structure (space group *P-62 m*), which contains two metallic (3*f* and 3*g*) and two non-metallic (2*c* and 1*b*) crystallographic sites [4]. The ferromagnetic transition in these alloys is coupled to discontinuous changes in the lattice parameters without a symmetry change, i.e. showing a magnetoelastic transition [4]. The synchrotron x-ray diffraction and absorption experiments as well as density functional theory (DFT) calculations reveal a significant redistribution of electron density concomitant to the magnetoelastic transition [5]. Consequently, apart from the magnetic and structural entropy changes, the electronic entropy change also greatly contributes to the total entropy changes and thus leads to the giant MCE in the (Mn,Fe)$_2$(P,Si) alloys [5,6].

The (Mn,Fe)$_2$(P,Si) alloys show undesirable thermal hysteresis (ΔT_{hys}) due to the structural discontinuity accompanied with the magnetoelastic transition [7], which limits the reversibility of the thermal cycles. Besides that, the giant MCE in the (Mn,Fe)$_2$(P,Si) alloys is usually observed in a narrow temperature range in the vicinity of the Curie temperature (T_C), which determines the operation temperature for the magnetic refrigeration and energy conversion applications [8]. As a result, many efforts have been made to diminish the ΔT_{hys} as well as to tune the T_C of the (Mn,Fe)$_2$(P,Si) alloys. Thang et al. [9] show that the ΔT_{hys} can be reduced through optimizing the heat treat parameters. The underlying mechanism actually lies on the variation of the stoichiometry of the (Mn,Fe)$_2$(P,Si) phase since the amounts of the impurity phases changes with the heat treatment conditions [9]. Dung et al. [2,10] found that by varying the Mn/Fe and P/Si ratios one can reduce the ΔT_{hys} and tailor the T_C of the (Mn,Fe)$_2$(P,Si) alloys. The addition of small atoms, such as boron [11] and carbon [12,13] also offers an effective way to diminish the ΔT_{hys} and tune the T_C. The 3*d* transition metal substitution can also tailor the magnetoelastic transition of the (Mn,Fe)$_2$(P,Si) alloys. The V, Co and Ni substitution decreases the ΔT_{hys}, while the Cu substitution has opposing effects [14,15]. Besides that, Wada et al. [16] reported that the replacement of the Fe by the 4*d* transition metal Ru, can also significantly reduce the

* Corresponding author.
** Corresponding author.
E-mail addresses: xuefeimiao@njust.edu.cn (X. Miao), xufeng@njust.edu.cn (F. Xu).

https://doi.org/10.1016/j.intermet.2019.106602
Received 1 July 2019; Received in revised form 21 August 2019; Accepted 27 August 2019
Available online 30 August 2019

ΔT_{hys} of the $(Mn,Fe)_2(P,Si)$ alloys. Nevertheless, at least 12.5 at.% of the Fe need to be replaced by the noble metal Ru in order to obtain a ΔT_{hys} value of around 3 K [16]. In the present work, we show that the substitution of the Fe by the Nb, an early 4*d* transition metal, provides an economical and effective way to manipulate the magnetoelastic transition of the $(Mn,Fe)_2(P,Si)$ alloys. The replacement of the Fe by merely 4.7 at.% Nb (i.e. $x = 0.04$) dramatically diminishes the thermal hysteresis from 10 to 1 K, while the giant MCE is retained.

2. Experimental details

Polycrystalline samples with nominal compositions of $Mn_{1.1}Fe_{0.85-x}Nb_xP_{0.43}Si_{0.57}$ (x = 0, 0.02, 0.03 and 0.04) were prepared by high-energy ball milling. Appropriate amounts of Mn, Fe, Nb, red P and Si powders with a purity higher than 99.8 wt% were mixed and ball milled at a speed of 400 rpm for 10 h. The ball-milled powders were pressed into tablets and then sealed into quartz ampoules in vacuum. The sealed tablets were annealed at 1373 K for 40 h before being quenched into iced water. The x-ray diffraction (XRD) patterns were collected on a PANalytical X-pert Pro diffractometer with Cu K_α radiation. This diffractometer is equipped with an Anton Paar TTK450 low-temperature chamber, which allows temperature-dependent XRD measurements. Structure refinement of the XRD patterns was performed using Fullprof's [17] implementation of the Rietveld refinement method. The morphology and element distribution of the samples were characterized using a field-emission scanning electron microscope (ZEISS, Sigma 500) with an x-ray energy dispersive spectroscope (EDS). The magnetic properties were measured using a physical property measurement system (PPMS, Quantum Design, Dynacool) with a vibrating sample magnetometer (VSM) module. The isothermal magnetization measurements were performed using the so-call "loop protocol" [18] to avoid the thermal-history effect. The specific heat was measured in different magnetic fields (0–1.5 T) using a home-built differential scanning calorimeter (DSC) in Delft University of Technology. The temperature of the sample can be varied between 240 and 320 K at a sweeping rate of 2 $Kmin^{-1}$. The error on the measured specific heat is less than 70 $Jkg^{-1}K^{-1}$. It should be noted that the samples for magnetization, specific heat and XRD measurements were pre-cycled in liquid nitrogen in order to get rid of the so-called "virgin effect" [19–21]. The SEM and EDS measurements were performed on initial samples without pre-cycling.

3. Results and discussion

The temperature-dependent magnetization (M) of the $Mn_{1.1}Fe_{0.85-x}Nb_xP_{0.43}Si_{0.57}$ alloys measured in 0.1 T is presented in Fig. 1(a). The T_C of the magnetoelastic transition decreases almost linearly with the Nb content by approximately 11.6 K per at.% of the Nb substitution. The effect of the Nb substitution on the T_C is stronger than that of the 3*d* metals (e.g. Cu, Co and Ni) which reduces the T_C by about 4.3–11.2 K per at.% of the 3*d* metals [14,15]. A clear thermal hysteresis (ΔT_{hys}), manifested by the difference in the T_C between the cooling and warming branches, has been observed for all the samples. Similar behavior is also observed in the temperature-dependent specific heat (c_p) curves in Fig. 1(b), suggesting a first-order transition character for all the samples. The large ΔT_{hys} value of approximately 10 K in the Nb-free sample has been significantly reduced to 4.5 K in the $x = 0.02$ sample. With an increase in Nb content to 0.03 and 0.04, the ΔT_{hys} can be further reduced to 2 and 1 K, respectively, suggesting the weakening of the first-order transition character and the improved reversibility of the magnetoelastic transition. Consequently, the replacement of Fe by Nb not only offers an effective tool to manipulate the operation temperature but also benefits the reversibility of the magnetoelastic transition for the $(Mn,Fe)_2(P,Si)$ magnetocaloric alloys.

Fig. 2(a) and (b) displays the contour plots of the XRD patterns measured upon cooling for the Nb-free and $x = 0.04$ samples,

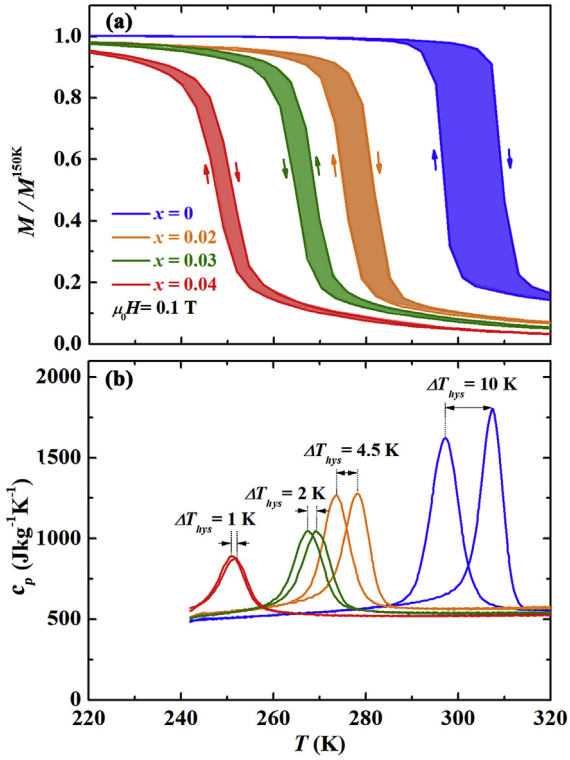

Fig. 1. Temperature dependence of (a) normalized magnetization measured in 0.1 T at a sweeping rate of 3 $Kmin^{-1}$ and (b) specific heat measured in 0 T at a sweeping rate of 2 $Kmin^{-1}$ for the $Mn_{1.1}Fe_{0.85-x}Nb_xP_{0.43}Si_{0.57}$ samples.

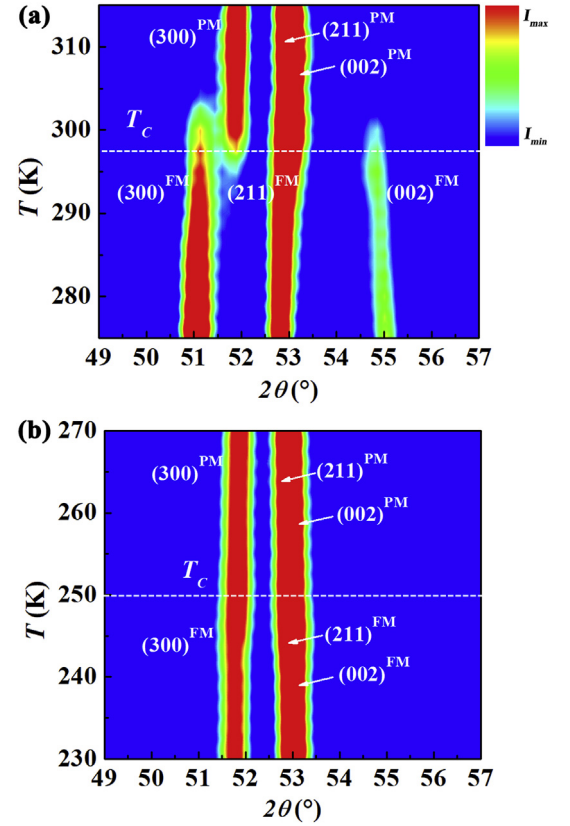

Fig. 2. Contour plots of the temperature-dependent XRD patterns for the $Mn_{1.1}Fe_{0.85-x}Nb_xP_{0.43}Si_{0.57}$ samples with $x = 0$ (a) and 0.04 (b). The bar on the right represents the normalized intensity scale.

respectively. The diffraction peaks show a clear discontinuity in the vicinity of the ferromagnetic transition temperature T_C for the Nb-free sample. One may notice that the (300) peak shifts to lower angles while the (002) peak moves to higher angles during the paramagnetic-ferromagnetic (PM-FM) transition upon cooling. This indicates the unit cell expands along the a axis while it contracts along the c axis during the PM-FM transition. There is no noticeable structural discontinuity in the contour plot of $x = 0.04$ sample, suggesting smaller lattice mismatch between the FM and PM phases. The relative changes in lattice parameters at T_C upon cooling are approximately 1.37% ($\Delta a/a$) and −2.86% ($\Delta c/c$) for the $x = 0$ sample, while these are 0.39% ($\Delta a/a$) and −0.48% ($\Delta c/c$) for the 0.04 samples. The strongly reduced lattice distortions in the $x = 0.04$ sample will cause smaller elastic strain energy and a lower energy barrier for the first-order magnetoelastic transition [7]. Therefore, a smaller hysteresis of around 1 K has been observed in the $x = 0.04$ sample (see Fig. 1). Apart from the enhanced reversibility, we found that the $x = 0.04$ sample can keep intact after thermal cycles using liquid nitrogen, revealing an improved mechanical stability. In contrast, the $x = 0$, 0.02 and 0.03 bulk samples break apart after thermal cycles in liquid nitrogen.

Fig. 3(a) and (b) illustrate the Arrot plots derived from the isothermal magnetization curves in the vicinity of the T_C for $x = 0$ and 0.04 samples. The S-shaped curves, reflecting relevant high-order terms in the Landau free energy expansion [22], further prove the first-order phase transition nature for both samples. One may notice that the S-shaped character of the Arrot plot is less pronounced for $x = 0.04$ sample, indicating that $x = 0.04$ samples may have a composition close to the border between the first- and second-order transitions, i.e. the tricritical point [23]. The samples in the vicinity of the tricritical point are expected to show a combination of a giant MCE, large reversibility and good mechanical stability [23–26].

The lattice parameters at 200 K derived from the XRD patterns are plotted as a function of the Nb content in Fig. 4(a). It should be noted

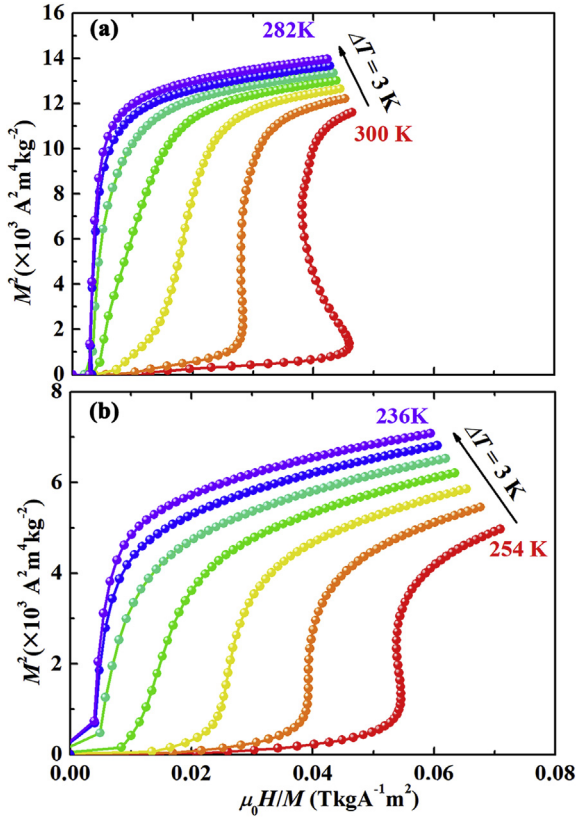

Fig. 3. The Arrot plots for the $Mn_{1.1}Fe_{0.85-x}Nb_xP_{0.43}Si_{0.57}$ samples with $x = 0$ (a) and 0.04 (b) derived from isothermal magnetization curves.

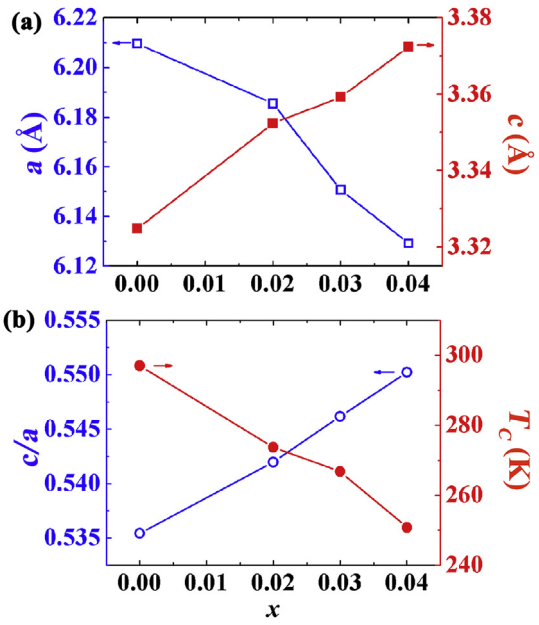

Fig. 4. (a) The lattice parameters at 200 K derived from the Rietveld refinement of the XRD data. (b) The calculated c/a ratio and the T_C determined from the cooling branch of the DSC curves as a function of the Nb content.

that all the samples are in the FM state at 200 K (see Fig. 1(a)). With an increase in the Nb content, the lattice parameter a is decreased while the lattice parameter c is increased. The anisotropic changes in the lattice parameters imply that the substitution of Fe with Nb atoms brings not only the size effect (i.e., Nb has a larger radius than Fe) but also variations in the chemical bonding and electronic redistribution. Fig. 4(b) shows c/a ratio and T_C as a function of the Nb content. The increase in c/a ratio is associated with the decrease in T_C for the $Mn_{1.1}Fe_{0.85-x}Nb_xP_{0.43}Si_{0.57}$ alloys, reflecting strong interaction between the lattice and spin degrees of freedom. A similar dependence of T_C on c/a ratio has also been observed in other $(Mn,Fe)_2(P,Si)$-type magnetocaloric materials [1,13,26,27]. Previous neutron/x-ray diffraction and first-principles calculations revealed that the magnetoelastic transition is associated with a metamagnetic transition of the Fe atom [5,28,29]. In the paramagnetic state, the valence electrons of Fe atoms are hybridized with neighboring Si atoms on the same ab plane [5]. During the ferromagnetic transition, the unit cell expands within the ab plane (see Fig. 2(a)), which destabilizes the chemical bonding between Fe and Si atoms and thus favors the moment formation of Fe atoms. As a result, Fe atoms experience a low-to high-moment transition (i.e., a metamagnetic transition) during the PM-FM magnetoelastic transition [5]. The different approaches of tuning the T_C in the $(Mn,Fe)_2(P,Si)$-type materials can essentially be attributed to the same origin, i.e., tailoring the metamagnetic behavior of Fe atoms. For instance, the increasing c/a ratio with increasing Nb content (see Fig. 4(b)) in the present study reflects the shortening of the Fe–Si distances in the ab plane, which favors the covalent bonding between the neighboring Fe and Si atoms. Therefore, the Nb substitution stabilizes the high-temperature PM phase and thus shifts T_C to lower temperatures.

Fig. 5(a) shows a SEM backscattered electrons (BSE) image from the $Mn_{1.1}Fe_{0.81}Nb_{0.04}P_{0.43}Si_{0.57}$ sample. One can observe some microcracks in the SEM image. It should be noted that the T_C of this sample is far below room temperature. Therefore, these microcracks probably originate from quenching after high-temperature annealing. Some narrow dark areas are observed between the large bright areas. The different contrast in the SEM BSE image reflects the variations in the average atomic mass as well as the surface morphology in the sample. Fig. 5(b)–(f) display the EDS maps of the Mn, Fe, Nb, P and Si in the same area as in Fig. 5(a). The Mn element is almost homogeneously

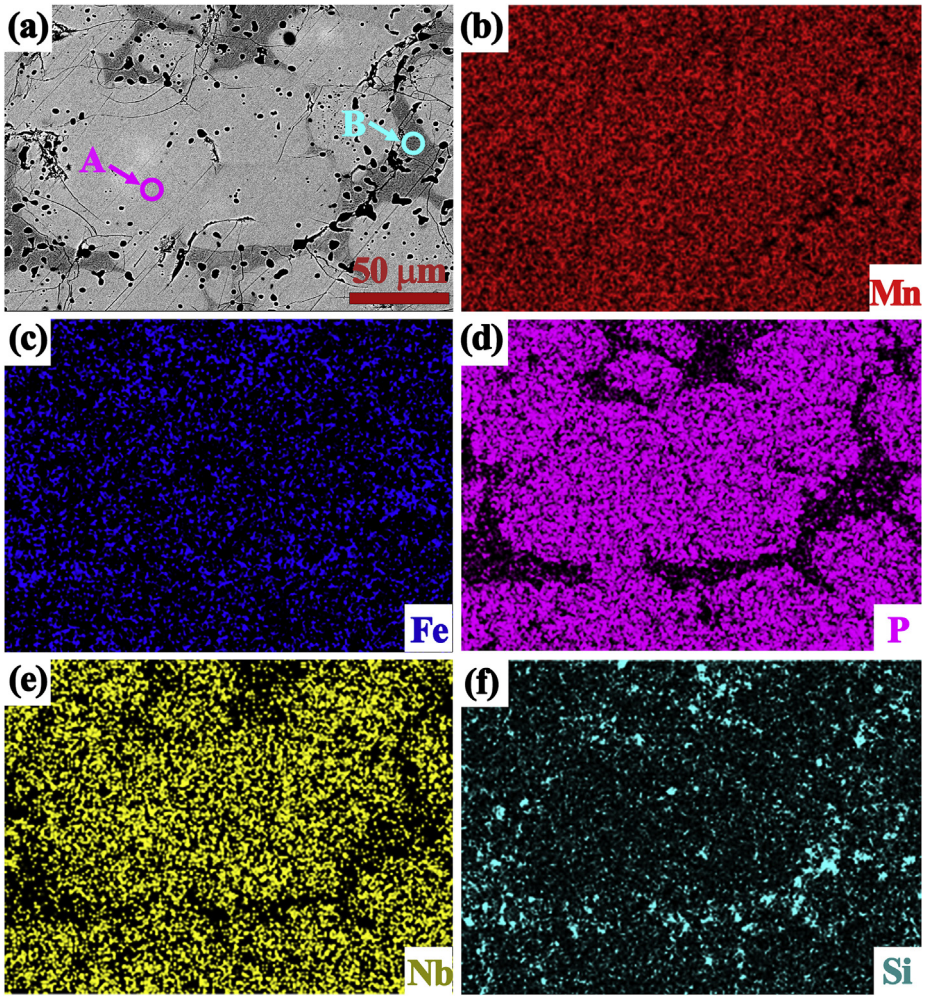

Fig. 5. (a) SEM BSE image and (b–f) the corresponding EDS maps for the $Mn_{1.1}Fe_{0.81}Nb_{0.04}P_{0.43}Si_{0.57}$ sample.

Table 1
Element concentrations detected by EDS for the regions marked by "A" and "B" in Fig. 5(a) from the $Mn_{1.1}Fe_{0.81}Nb_{0.04}P_{0.43}Si_{0.57}$ sample.

	Region A	Region B
Mn (at.%)	39.24 ± 0.22	40.23 ± 0.21
Fe (at.%)	26.02 ± 0.20	35.18 ± 0.21
Nb (at.%)	1.56 ± 0.12	0.15 ± 0.10
P (at.%)	14.83 ± 0.17	2.24 ± 0.09
Si (at.%)	18.34 ± 0.15	22.20 ± 0.17

distributed in the whole sample, while other elements show some concentration variations between the dark and light areas in Fig. 5(a). The dark areas are deficient in Nb and P elements, while they are rich in Fe and Si elements. The relative concentration of each element in the bright and dark areas, detected from the spots marked by "A" and "B", respectively, has been summarized in Table 1. The bright area in Fig. 5(a) corresponds to the Fe_2P-type main phase with a measured composition of $Mn_{1.17}Fe_{0.78}Nb_{0.05}P_{0.45}Si_{0.55}$, which is close to the nominal composition. The dark area is from the Fe_3Si-based secondary phase with a measured composition of $Mn_{1.60}Fe_{1.40}Nb_{0.01}P_{0.09}Si_{0.91}$, which is commonly observed in the $(Mn,Fe)_2(P,Si)$-based alloys [30–32]. Consequently, the XRD and EDS results indicate that the Nb atoms have entered the $(Mn,Fe)_2(P,Si)$ lattice, which are responsible for the observed changes in the magnetoelastic transition.

The magnetocaloric properties can be quantitatively characterized by the isothermal entropy Δs_T and the adiabatic temperature change ΔT_{ad}. The former determines the maximum heat to be taken from a load, while the latter represents the maximum temperature span to be realized between a load and a heat sink. The Δs_T and the ΔT_{ad} of the samples can be derived from the field-dependent specific heat measurements based on the following equations [33]:

$$\Delta s_T(T, \Delta H) = \int_0^T \frac{c_p(T,\ H_f)}{T} dT - \int_0^T \frac{c_p(T,\ H_i)}{T} dT \quad (1)$$

$$\Delta T_{ad} \cong -\frac{T}{c_p(T,\ H_f)} \Delta s_T(T, \Delta H) \quad (2)$$

where the $c_p(T, H_f)$ and $c_p(T, H_i)$ represent the temperature-dependent specific heat measured at magnetic fields of H_f and H_i, respectively.

The specific heat measurements were performed at different magnetic fields (from 0 to 1.5 T) in the temperature range between 240 and 320 K for the $Mn_{1.1}Fe_{0.85-x}Nb_xP_{0.43}Si_{0.57}$ alloys. Fig. 6(a) and (b) show the Δs_T and the ΔT_{ad} at different temperatures, respectively, derived from the in-field DSC data based on Eqs. (1) and (2). With an increase in the Nb content, both Δs_T and the ΔT_{ad} are reduced due to the weakening of the first-order magnetoelastic transition. Nevertheless, the Δs_T values of all the samples are at least twice larger than that of the benchmark magnetocaloric material Gd [34], while the ΔT_{ad} values are comparable to that of the Gd. Besides that, the $Mn_{1.1}Fe_{0.82}Nb_{0.03}P_{0.43}Si_{0.57}$ alloy exhibits superior Δs_T and ΔT_{ad} values in a field change of 1 T than the 3*d* metal-substituted (e.g., Co, Ni [14,35]) and the Ru-substituted $(Mn,Fe)_2(P,Si)$ alloys [16] with a similar ΔT_{hys} value.

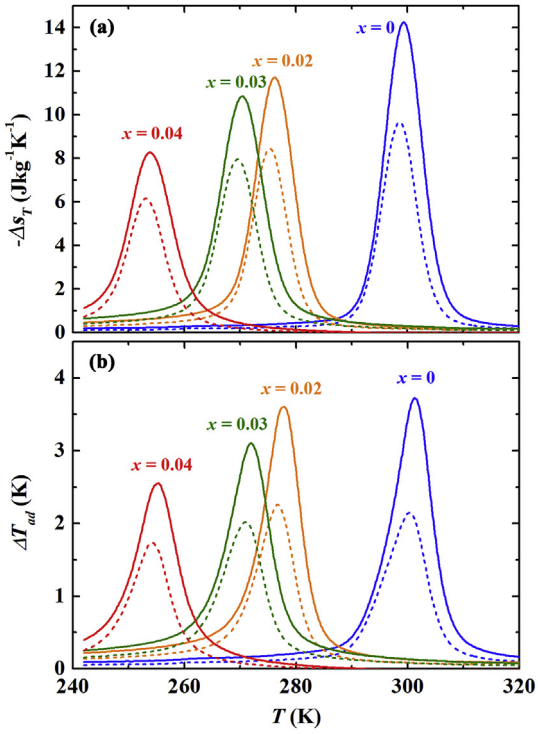

Fig. 6. (a) Isothermal entropy change and (b) adiabatic temperature change for a field change of 1 (dashed curves) and 1.5 T (solid curves) for the $Mn_{1.1}Fe_{0.85-x}Nb_xP_{0.43}Si_{0.57}$ samples.

4. Conclusions

In summary, based on comprehensive magnetometric, in-field calorimetric, in-situ x-ray diffractometric and electron microscopic studies, we found that the Nb substitution for Fe has a significant influence on the structure, magnetoelastic transition and magenetocaloric properties of the $(Mn,Fe)_2(P,Si)$ alloys. The 4*d* metal element Nb can replace the Fe atoms in the hexagonal lattice. This leads to anisotropic changes in the unit cell parameters, i.e. a contraction along the *a* axis and an expansion along the *c* axis. The ferromagnetic transition of the $(Mn,Fe)_2(P,Si)$ alloys are effectively manipulated by Nb substitution due to a strong coupling between lattice and spin degrees of freedom. With an increase in Nb content, the undesirable hysteresis and structural discontinuity can be significantly reduced while the giant magnetocaloric properties are still retained. As a result, the Nb-containing samples show better reversibility of the magnetoelastic transition as well as enhanced mechanical stability. The small hysteresis, tailorable operation temperature, giant magnetocaloric effect and improved mechanical stability make the Nb-containing $(Mn,Fe)_2(P,Si)$ alloys promising for commercial magnetic refrigeration and energy conversion applications.

Conflicts of interest

The authors declare no conflicts of interest.

Acknowledgements

This work was supported by the National Natural Science Foundation of China (grant numbers 51801102, U1832191); the Natural Science Foundation of Jiangsu Province (grant number BK20180491); and the Open Fund of Large Facilities in Nanjing University of Science and Technology.

References

[1] N.H. Dung, Z.Q. Ou, L. Caron, L. Zhang, D.T.C. Thanh, G.A. de Wijs, R.A. de Groot, K.H.J. Buschow, E. Brück, Adv. Energy Mater. 1 (2011) 1215–1219.
[2] N.H. Dung, L. Zhang, Z.Q. Ou, E. Brück, Scr. Mater. 67 (2012) 975–978.
[3] O. Tegus, E. Brück, K.H.J. Buschow, F.R. de Boer, Nature 415 (2002) 150.
[4] X.F. Miao, L. Caron, P. Roy, N.H. Dung, L. Zhang, W.A. Kockelmann, R.A. de Groot, N.H. van Dijk, E. Brück, Phys. Rev. B 89 (2014) 174429.
[5] M.F.J. Boeije, P. Roy, F. Guillou, H. Yibole, X.F. Miao, L. Caron, D. Banerjee, N.H. van Dijk, R.A. de Groot, E. Brück, Chem. Mater. 28 (2016) 4901–4905.
[6] D. Bessas, M. Maschek, H. Yibole, J.W. Lai, S.M. Souliou, I. Sergueev, A.I. Dugulan, N.H. van Dijk, E. Brück, Phys. Rev. B 97 (2018) 094303.
[7] X.F. Miao, H. Sepehri-Amin, K. Hono, Scr. Mater. 138 (2017) 96.
[8] E. Brück, N.T. Trung, Z.Q. Ou, K.H.J. Buschow, Scr. Mater. 67 (2012) 590–593.
[9] N.V. Thang, H. Yibole, N.H. van Dijk, E. Brück, J. Alloy. Comp. 699 (2017) 633–637.
[10] N.H. Dung, L. Zhang, Z.Q. Ou, E. Brück, Appl. Phys. Lett. 99 (2011) 092511.
[11] F. Guillou, G. Porcari, H. Yibole, N.H. van Dijk, E. Brück, Adv. Mater. 26 (2014) 2671.
[12] X.F. Miao, N.V. Thang, L. Caron, H. Yibole, R.I. Smith, N.H. van Dijk, E. Brück, Scr. Mater. 124 (2016) 129.
[13] Q. Zhou, Z.G. Zheng, W.H. Wang, L. Lei, A. He, D.C. Zeng, Intermetallics 106 (2019) 94–99.
[14] Z.Q. Ou, N.H. Dung, L. Zhang, L. Caron, E. Torun, N.H. van Dijk, O. Tegus, E. Brück, J. Alloy. Comp. 730 (2018) 392–398.
[15] J. Lai, B. Huang, X.F. Miao, N. van Thang, X. You, M. Maschek, L. van Eijck, D. Zeng, N.H. van Dijk, E. Brück, J. Alloy. Comp. (2019), https://doi.org/10.1016/j.jallcom.2019.06.239.
[16] H. Wada, K. Nakamura, K. Katagiri, T. Ohnishi, K. Yamashita, A. Matsushita, Jpn. J. Appl. Phys. 53 (2014) 063001.
[17] J. Rodriguez-Carvajal, Physica B 192 (1993) 55–69.
[18] L. Caron, Z.Q. Ou, T.T. Nguyen, D.T. Cam Thanh, O. Tegus, E. Brück, J. Magn. Magn. Mater. 321 (2009) 3559–3566.
[19] M. Fries, L. Pfeuffer, E. Bruder, T. Gottschall, S. Ener, L.V.B. Diöp, T. Grob, K.P. Skokov, O. Gutfleisch, Acta Mater. 132 (2017) 222–229.
[20] A. Bartok, M. Kustov, L.F. Cohen, A. Pasko, K. Zehani, L. Bessais, F. Mazaleyrat, M. LoBue, J. Magn. Magn. Mater. 400 (2016) 333–338.
[21] X.F. Miao, L. Caron, Z. Gercsi, A. Daoud-Aladine, N.H. van Dijk, E. Brück, Appl. Phys. Lett. 107 (2015) 042403.
[22] L. Landau, Zh. Eksp. Teor. Fiz. 7 (1937) 19–32.
[23] K. Morrison, J. Moore, K. Sandeman, A. Caplin, L. Cohen, Phys. Rev. B 79 (2009) 134408.
[24] X.F. Miao, S.H. Hu, F. Xu, E. Brück, Rare Met. 37 (2018) 723–733.
[25] F. Guillou, H. Yibole, N.H. van Dijk, L. Zhang, V. Hardy, E. Brück, J. Alloy. Comp. 617 (2014) 569.
[26] N.V. Thang, X.F. Miao, N.H. van Dijk, E. Brück, J. Alloy. Comp. 670 (2016) 123.
[27] D.M. Liu, H. Zhang, S.B. Wang, W.Q. Xiao, Z.L. Zhang, N. Tian, C.X. Liu, M. Yue, Q.Z. Huang, J.X. Zhang, J.W. Lynn, J. Alloy. Comp. 633 (2015) 120–126.
[28] X.F. Miao, Y. Mitsui, A.I. Dugulan, L. Caron, N.V. Thang, P. Manuel, K. Koyama, K. Takahashi, N.H. van Dijk, E. Brück, Phys. Rev. B 94 (2016) 094426.
[29] N.H. Dung, L. Zhang, Z.Q. Ou, L. Zhao, L. van Eijck, A.M. Mulders, M. Avdeev, E. Suard, N.H. van Dijk, E. Brück, Phys. Rev. B 86 (2012) 045134.
[30] M. Fries, L. Pfeuffer, E. Bruder, T. Gottschall, S. Ener, L.V.B. Diop, T. Gröb, K.P. Skokov, O. Gutfleisch, Acta Mater. 132 (2017) 222.
[31] Z.G. Zheng, Z.C. Tan, H.Y. Yu, J.L. Zhang, D.C. Zeng, V. Franco, Mater. Res. Bull. 77 (2016) 29–34.
[32] M.Y. Wu, X.R. Yang, R.X. Zou, F. Qian, S.Y. Hu, W.Y. Wang, G.L. Zhong, X.F. Miao, F. Xu, Mater. Lett. 236 (2019) 579–582.
[33] A. Smith, C.R.H. Bahl, R. Bjørk, K. Engelbrecht, K.K. Nielsen, N. Pryds, Adv. Energy Mater. 2 (2012) 1288–1318.
[34] J. Gschneidner, K. A, V.K. Pecharsky, A.O. Tsokol, Rep. Prog. Phys. 68 (2005) 1479–1539.
[35] N.V. Thang, N.H.V. Dijk, E. Brück, Materials 10 (2016) 14.